Draft version September 8, 2016
Preprint typeset using LaTeX style emulateapj v. 5/2/11

arXiv:1609.01955v1 [astro-ph.SR] 7 Sep 2016

PROTON HEATING BY PICK-UP ION DRIVEN CYCLOTRON WAVES IN THE OUTER HELIOSPHERE: HYBRID EXPANDING BOX SIMULATIONS

Petr Hellinger[1,2] and Pavel M. Trávníček[1–3]

Draft version September 8, 2016

ABSTRACT

Using one-dimensional hybrid expanding box model we investigate properties of the solar wind in the outer heliosphere. We assume a proton-electron plasma with a strictly transverse ambient magnetic field and, beside the expansion, we take into account influence of a continuous injection of cold pick-up protons through the charge-exchange process between the solar wind protons and hydrogen of interstellar origin. The injected cold pick-up protons form a ring distribution function that rapidly becomes unstable and generate Alfvén cyclotron waves. The Alfvén cyclotron waves scatter pick-up protons to a spherical shell distribution function that thickens over that time owing to the expansion-driven cooling. The Alfvén cyclotron waves heat solar wind protons in the perpendicular direction (with respect to the ambient magnetic field) through the cyclotron resonance. At later times, the Alfvén cyclotron waves become parametrically unstable and the generated ion acoustic waves heat protons in the parallel direction through the Landau resonance. The resulting heating of the solar wind protons is efficient on the expansion time scale.

1. INTRODUCTION

Properties of the solar wind plasma in the outer heliosphere are importantly influenced by inelastic collisions between ions and neutrals of interstellar origin (Burlaga et al. 1996; Zank et al. 2009; Richardson & Stone 2009). The solar wind ions and interstellar neutrals interact through the charge-exchange process. The neutrals (mostly hydrogen) become ionized and the interaction between the newly created, pick-up ions and the ambient solar wind plasma leads to a deceleration of the solar wind and has likely an important effect on ion thermal energetics (Richardson et al. 1995; Wang et al. 2000; Richardson et al. 2008). The nonthermal pick-up ions play likely an important role at the termination shock (Burlaga et al. 2008; Decker et al. 2008). The actual form of the pick-up ion distribution function just upstream from the termination shock importantly influences the shock properties and ion acceleration (Giacalone & Decker 2010; Matsukiyo & Scholer 2014; Yang et al. 2015).

A pick-up ion dominated distant solar wind can be to some extend described using a macroscopic multi-fluid approach (Zank et al. 2014). Global multi-fluid simulations show that the interaction between solar wind and interstellar neutrals has an important effect on the global properties of the outer heliosphere (e.g., Usmanov et al. 2012). However, the highly nonthermal newly born pick-up ion population leads naturally to plasma instabilities where strongly kinetic processes such as the cyclotron and Landau resonances are expected (Gary 1993). Depending on the orientation of the background magnetic field, the pick-up have different distribution functions (Zank & Cairns 2000). A ring distribution function is generated by injection perpendicular to the ambient solar wind. Such a distribution has an effective perpendicular temperature anisotropy and may generate Alfvén cyclotron waves (or mirror instabilities, etc.); the generated waves scatter the ring pick-up protons to a spherical shell-like velocity distribution function (Lee & Ip 1987; Williams & Zank 1994) and may heat directly the solar wind protons through the cyclotron instability (Gray et al. 1996; Richardson et al. 1996). Injection parallel to the ambient magnetic field leads to several beam-type instabilities (Daughton & Gary 1998). For a general orientation of the ambient magnetic field a ring-beam distribution function is generated and both the temperature anisotropy and the differential velocity could be a source of free energy for kinetic instabilities (Vandas & Hellinger 2015). The pick-up ion driven instabilities are active in the solar wind as indicated by in situ observation of the generated waves (Joyce et al. 2010; Cannon et al. 2014b,a; Aggarwal et al. 2016).

The linear and nonlinear studies of pick-up ion driven instabilities usually assume a homogeneous plasma that is at odds with ubiquitous turbulent fluctuations observed in the distant solar wind (Fraternale et al. 2016). In situ observations of enhanced wave activity (Joyce et al. 2010; Cannon et al. 2014b,a; Aggarwal et al. 2016) indicate that the pick-up ion driven instabilities are active in the solar wind. This is supported by direct hybrid simulations of Hellinger et al. (2015) showing that kinetic instabilities may coexist with turbulence. The wave activity generated by pick-up ions may be a local source of turbulence as assumed in phenomenological transport models of turbulence (Zank et al. 1996; Matthaeus et al. 1999; Isenberg et al. 2003; Smith et al. 2006; Isenberg et al. 2010; Adhikari et al. 2015); the enhanced level of turbulence leads to enhanced cascade and heating rates. However, connection between turbulence and kinetic instabilities driven by non-thermal particle velocity distribution functions is far from being understood.

In this paper we investigate long-time evolution of the expanding solar wind plasma under the effect of a con-

petr.hellinger@asu.cas.cz
[1] Astronomical Institute, CAS, Bocni II/1401, CZ-14100 Prague, Czech Republic
[2] Institute of Atmospheric Physics, CAS, Bocni II/1401, CZ-14100 Prague, Czech Republic
[3] Space Sciences Laboratory, UCB, Berkeley, USA.

tinuous injection of pick-up protons. Section 2 describes the simulation method, the hybrid expanding box model. Section 3 presents the main simulation results. In section 4 we discuss the simulation results.

2. EXPANDING BOX MODEL

To study the response of the plasma to a slow expansion we use the expanding box model (Grappin et al. 1993; Liewer et al. 2001) implemented to the hybrid code (Matthews 1994; Hellinger et al. 2003). In the hybrid expanding box (HEB) model the expansion is described as an external force where a constant solar wind radial velocity v_{sw} is assumed. The radial distance R is then

$$R = R_0 + v_{sw}t = R_0\left(1 + \frac{t}{t_{e0}}\right) \tag{1}$$

where R_0 is an initial radial distance and $t_e = R_0/v_{sw}$ is the characteristic (initial) expansion time. The initial radial distance R_0 is one of the free parameters in the model. Here we assume a strictly transverse magnetic field and $R_0 \sim 10$ au. Transverse scales (with respect to the radial direction) of a small portion of plasma, co-moving with the solar wind velocity, increase with time $\propto (1 + t/t_{e0})$. The expanding box uses these co-moving coordinates, replacing the spatial dependence by the temporal one (see Equation (1)). The physical transverse scales of the simulation box increase with time (see Hellinger & Trávníček 2005, for a detailed description of the code) and the standard periodic boundary conditions are used.

The kinetic model uses the hybrid approximation, i.e., electrons are considered as a massless, charge neutralizing fluid, with a constant temperature; ions are described by a particle-in-cell model and are advanced by a Boris' scheme that requires the fields to be known at half time steps ahead of the particle velocities. This is achieved by advancing the current density to this time step with only one computational pass through the particle data at each time step (Matthews 1994). The characteristic spatial and temporal units used in the model are c/ω_{pp0} and $1/\omega_{cp0}$ respectively, where c is the speed of light, $\omega_{pp0} = (n_{p0}e^2/m_p\epsilon_0)^{1/2}$ is the initial proton plasma frequency, and $\omega_{cp0} = eB_0/m_p$ is the initial proton gyrofrequency (B_0: the initial magnitude of the ambient magnetic field $\boldsymbol{B}_0$, n_{p0} is the initial proton density, e and m_p are the proton electric charge and mass, respectively; finally, ϵ_0 is the dielectric permittivity of vacuum). We use the spatial resolution $\Delta x = 0.25c/\omega_{pp0}$, and there are initially 131,072 particles per cell for the solar wind protons. Fields and moments are defined on a 1-D (periodic) grid with 8192 points. Protons are advances using a time step $\Delta t = 0.05/\omega_{cp0}$, while the magnetic field $\boldsymbol{B}$ is advanced with a smaller time step $\Delta t_B = \Delta t/10$. The initial ambient magnetic field is directed along the (transverse) x direction, parallel to the ambient magnetic field $\boldsymbol{B}_0 = (B_0, 0, 0)$, and we impose a continuous expansion in x and z directions with the characteristic time $t_e = 10^4/\omega_{cp0}$. The radial direction is in the y direction. The expansion leads to a decrease of the density as $(1 + t/t_e)^{-2}$ whereas the magnitude of the magnetic field decreases as $(1 + t/t_e)^{-1}$ for the strictly transverse magnetic field.

In the simulation pick-up protons are continuously injected (cf. Cowee et al. 2008). The injection mechanism is the charge exchange between interstellar neutrals and the solar wind protons. For the sake of simplicity we assume that the charge exchange is energy/velocity independent. For the loss rate of the incident solar wind protons with the distribution function f_p we have

$$\left(\frac{\mathrm{d}f_p}{\mathrm{d}t}\right)_{cx} = -\nu_{cx}f_p \tag{2}$$

where the charge-exchange frequency ν_{cx} is taken to be $\nu_{cx} = 10^{-6}\omega_{cp0}$. The characteristic charge-exchange time $t_{cx} = 1/\nu_{cx}$ is 100 times longer than the expansion time t_e. The solar wind protons that are lost through the charge-exchange process are removed from the simulation (but their velocities are stored) and replaced by cold pick-up protons with the mean radial velocity $v_R = -10v_A \sim -v_{sw}$. The charge-exchange process, Equation (2), leads to the decrease of the solar wind proton number density (with respect to the electron one) as $n_p/n_e \propto \exp(-\nu_{cx}t)$ (note that at the same time the particle number densities decrease owing to the expansion). At the end of the simulation at $8t_e$ there is about 8 % of pick-up protons. The injection of pick-up protons also decelerates the solar wind plasma. At the end of the simulation the solar wind protons are decelerated by about $0.75v_A$.

3. SIMULATION RESULTS

The chosen initial conditions are stable with respect to kinetic instabilities. The continuous injection of pick-up ions and the expansion tend to change the plasma properties creating a free energy for kinetic instabilities. Let us investigate the evolution of the HEB simulation starting with the wave activity.

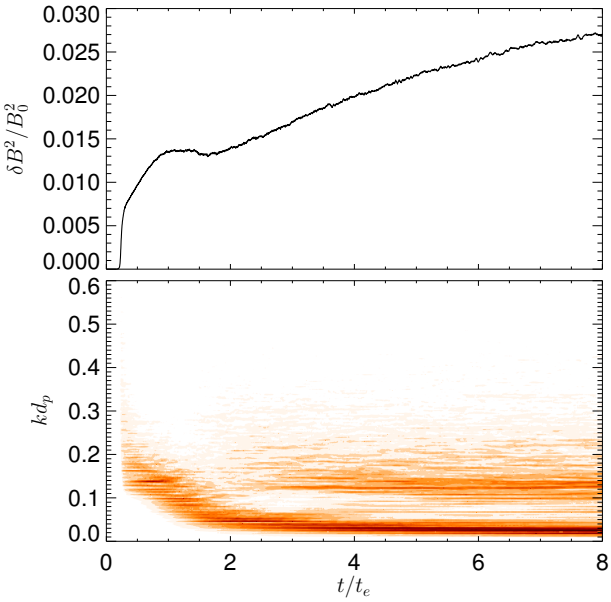

Figure 1. Evolution of fluctuating magnetic field: (top) δB^2 as a function of t; (bottom) color scale plot of δB^2 as a function of t and k.

Figure 1 shows an evolution of the fluctuating magnetic field (normalized to the ambient magnetic field)

$\delta B^2/B_0^2$ as a function of time (top panel). The bottom panel shows the color scale plot of the fluctuating magnetic field as a function of time and the wave vector k. Figure 1 shows that $\delta B/B_0$ and grows exponentially for $0.1t_e \lesssim t \lesssim 0.2t_e$. After the saturation δB grows secularly, i.e., about linearly in time, (cf., Matteini et al. 2006; Rosin et al. 2011; Kunz et al. 2014). Between $t_e \lesssim t \lesssim 2t_e$ there is another change of behavior, $\delta B/B_0$ remains about constant. For $t \gtrsim 2t_e$ $\delta B/B_0$ grows again in a secular manner. Bottom panel of Figure 1 shows that waves are initially generated with $0.1 \lesssim kd_\mathrm{p} \lesssim 0.2$. The fluctuating wave energy then shifts to smaller wave vectors (longer wavelengths) $kd_\mathrm{p} \sim 0.05$. For $t \gtrsim 2t_e$ there appears a secondary population of wave modes with $0.1 \lesssim kd_\mathrm{p} \lesssim 0.16$.

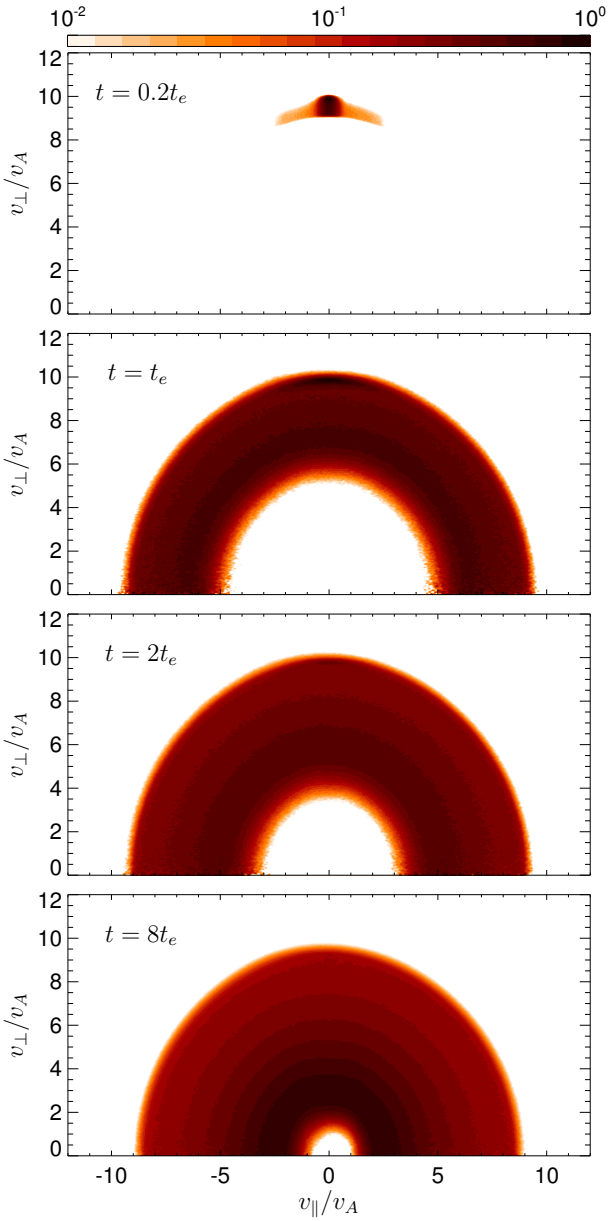

Figure 2. Evolution of the pick-up proton velocity distribution function (normalized to its maximum value) as a function of $v_\parallel$ and $v_\perp$ at $t = 0.2t_e$, t_e, $2t_e$, and $8t_e$ (from top to bottom). The color scale is shown on the top.

The observed wave activity is generated by the continuously injected pick-up protons that initially form a ring velocity distribution function (Vandas & Hellinger 2015). The ring velocity distribution function has a strong effective perpendicular temperature anisotropy that leads to generation of Alfvén ion cyclotron (AIC) waves (Gray et al. 1996) which in turn diffuse the ring ions. Figure 2 shows the evolution of the pick-up proton velocity distribution functions. At $t = 0.2t_e$, i.e., around the saturation of the initial exponential growth of the magnetic fluctuations the pick-up proton velocity distribution function takes shape of a partially diffused ring that is expected for the saturated level of a weak ring instability (cf., Florinski et al. 2010). The pick-up proton velocity distribution function exhibit a strong concentration of the newly born ions at the injection position, $v_\parallel \sim 0$ and $v_\perp \sim 10v_A$. At $t = t_e$ the pick-up proton velocity distribution exhibit a thick spherical shell velocity distribution function as well as diffused enhancement around the injection region $v_\parallel \sim 0$ and $v_\perp \sim 10v_A$. For a cold ring a thin spherical shell is expected but the expansion leads to an anisotropic cooling that transports the diffused pick-up protons to the regions with smaller velocities. At $t = 2t_e$ the pick-up protons exhibit a shell velocity distribution function further thickened owing to the expansion driven cooling. This trend continues till $t = 8t_e$, we observe no qualitative changes between $t = 2t_e$ and $t = 8t_e$.

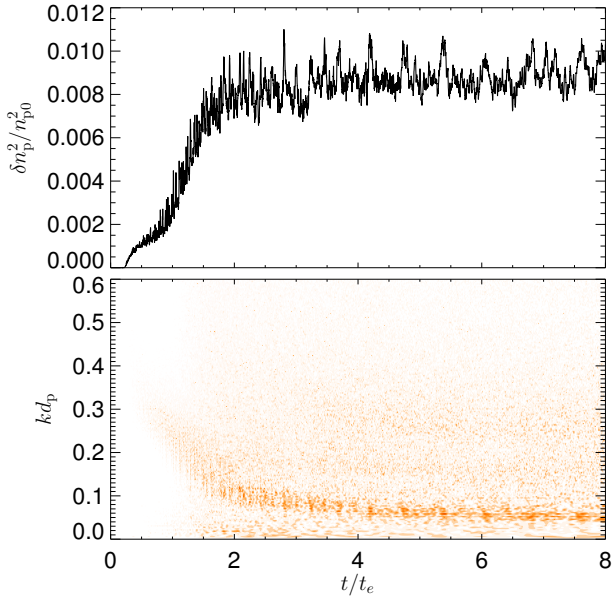

Figure 3. Evolution of the (core) proton density fluctuations: (top) δn_p^2 as a function of t; (bottom) color scale plots of (bottom) δn_p^2 as a function of k and t.

The appearance of a secondary population of wave modes indicates another, possible secondary instability. The AIC waves are prone to parametric instabilities (Hollweg 1994); the AIC waves couple to compressible ion acoustic modes and AIC waves with different wavelengths. Enhanced proton density fluctuations may be an indication of such a process. Figure 3 shows the (core) proton density fluctuations δn_p^2 (normalized to the background density n_p0) as a function of time (top panel).

The bottom panel shows the color scale plot of the fluctuating magnetic field as a function of time and the wave vector k. Figure 3 shows that weak density fluctuations appear during the exponential phase. This is due to the second order effects owing to ponderomotive force. After the saturation there is an exponential-like growth of the density fluctuations till $t \sim 1.5t_e$. The enhanced density fluctuations appear initially around $kd_\mathrm{p} \sim 0.1$ at $t = 2t_e$ and shift to smaller wave vectors at the time goes on.

Combination of Figures 1 and 3 suggests that the AIC waves generated by the pick-up protons become parametrically unstable and generate the ion acoustic waves and the secondary population of AIC waves. An additional, bi-coherence analysis (not shown here) indicate a weak phase coherence between the two AIC waves and the compressible modes. The phase coherence starts for $t \gtrsim t_e$ and is kept till $t = 8t_e$; it is important to note that the situation is symmetric with respect to the background magnetic field $\boldsymbol{B}_0$, the initial AIC waves are generated both parallel and anti-parallel to $\boldsymbol{B}_0$, the secondary AIC waves as well as the ion acoustic waves also appear both parallel and anti-parallel to $\boldsymbol{B}_0$. The presence of forward and backward propagating modes considerably complicates the phase coherence analysis. The actual nature of the parametric instability needs more work as the theoretical properties of parametric instabilities at ion kinetic scales are complicated (cf., Hollweg 1994; Vasquez 1995).

The ion acoustic modes interact through the Landau resonance with protons and lead to parallel acceleration/heating of the resonant particles (Araneda et al. 2008; Matteini et al. 2010). Figure 4 shows the evolution of the core proton velocity distribution functions. At $t = 0.2t_e$, i.e., around the saturation of the initial exponential growth of the magnetic fluctuations the solar wind protons are essentially unaffected by the AIC waves. At $t = t_e$ the solar wind protons exhibit signatures of perpendicular heating (and parallel cooling) through the cyclotron resonance with the AIC waves (for $|v_\parallel| \sim 0.3$–$0.6v_A$). At $t = 2t_e$ the solar wind proton distribution functions exhibit regions with an efficient parallel heating (for $|v_\parallel| \sim 0.3$–$0.7v_A$) owing to the Landau resonance with the compressible ion-acoustic waves.

The total proton distribution function consists of both the solar wind and pick-up ions. It's interesting to look at this total distribution function. Figure 5 shows the total one-dimensional velocity distribution function F (normalized to its maximum) as a function of v at $t = 0.2t_e$, t_e, $2t_e$, and $8t_e$ (from top to bottom). The one-dimensional distribution function F is obtained by integration of the three-dimensional total proton distribution function over the spherical angles $F = \int (f_\mathrm{p} + f_\mathrm{pui})\mathrm{d}\Omega$. Figure 5 shows in a more quantitative way the thickening of the pick-up ion shell. At the end of simulation (Figure 5, bottom panel) the one-dimensional distribution function F falls as $\propto v^{-1.4}$ between 3 and 8 v_A. We expect that the distribution function of pick-ups would eventually become a power-law like with a cut off at the injection velocity.

Macroscopic evolution of the simulated system is given in Figure 6 that compares the evolution of the solar wind proton temperatures (parallel, perpendicular, and total ones) compared to the double adiabatic/CGL prediction

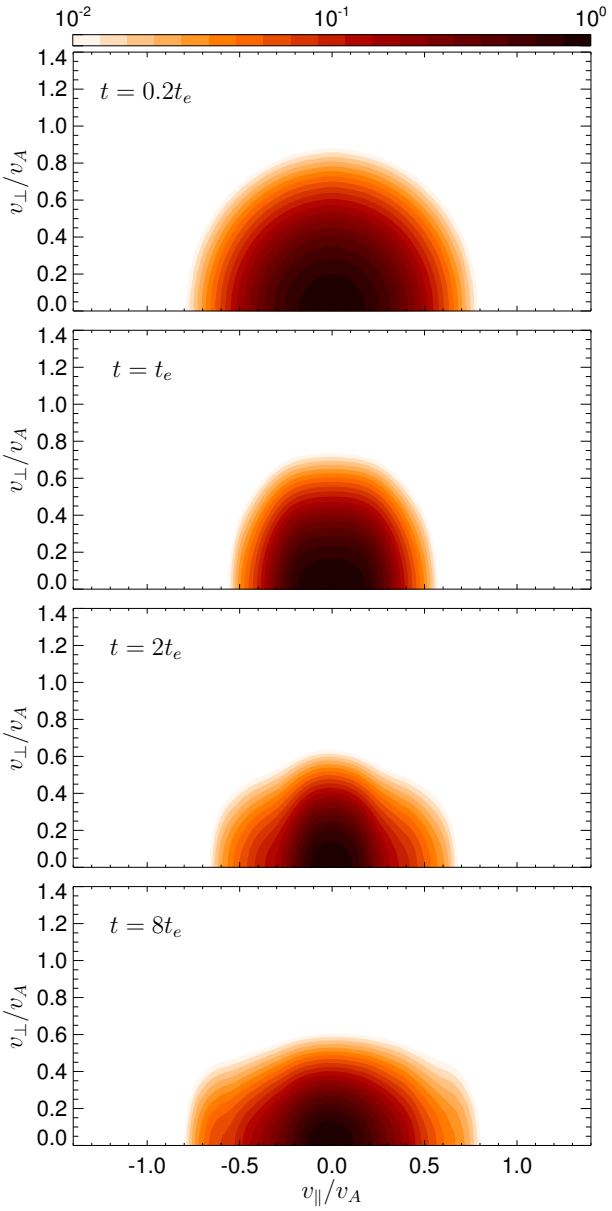

Figure 4. Evolution of the (core) proton velocity distribution function (normalized to its maximum value) as a function of $v_\parallel$ and $v_\perp$ at $t = 0.2t_e$, t_e, $2t_e$, and $8t_e$ (from top to bottom). The color scale is shown on the top.

(Chew et al. 1956)

$$T_{\mathrm{p}\parallel}\big|_{CGL} \propto \frac{n^2}{B^2} \quad \text{and} \quad T_{\mathrm{p}\perp}\big|_{CGL} \propto B \tag{3}$$

(and the adiabatic one $T_\mathrm{p}|_{adiab} \propto n^{2/3}$ for the total temperature). During the initial exponential growth of the magnetic fluctuations protons are cooled in the parallel direction and heated in the perpendicular direction as expected from the cyclotron resonance between protons and AIC waves (cf., Hollweg & Isenberg 2002); this cooling is also apparent in Figure 4 (at $t = t_e$). An efficient parallel heating appears later, $t \gtrsim t_e$, during the generation of enhanced density fluctuations due to the parametric instability in agreement of the microscopic properties of the proton velocity distribution function.

Finally, the numerical code keeps information about

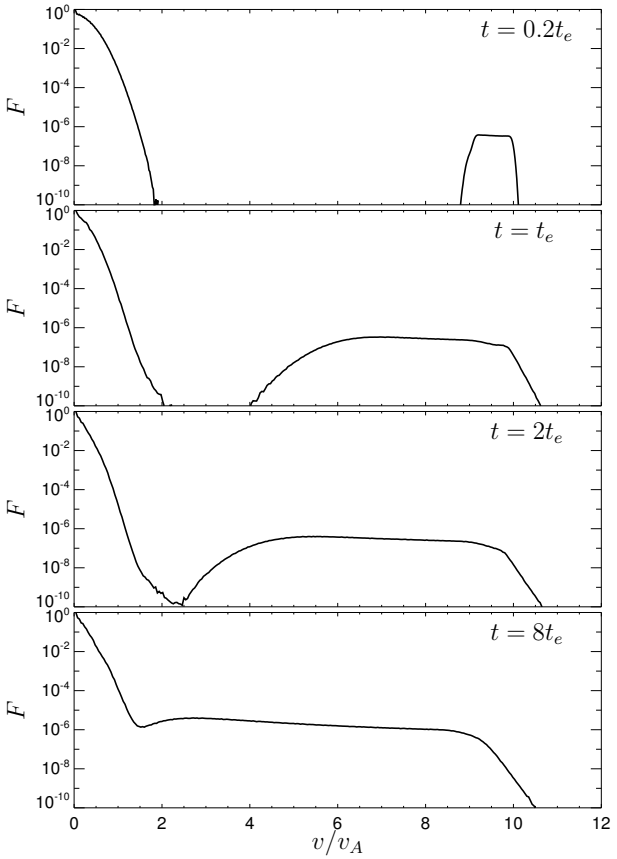

Figure 5. Evolution of the total (core solar wind + pick-up protons) one-dimensional distribution function as a function of v at $t = 0.2t_e$, t_e, $2t_e$, and $8t_e$ (from top to bottom).

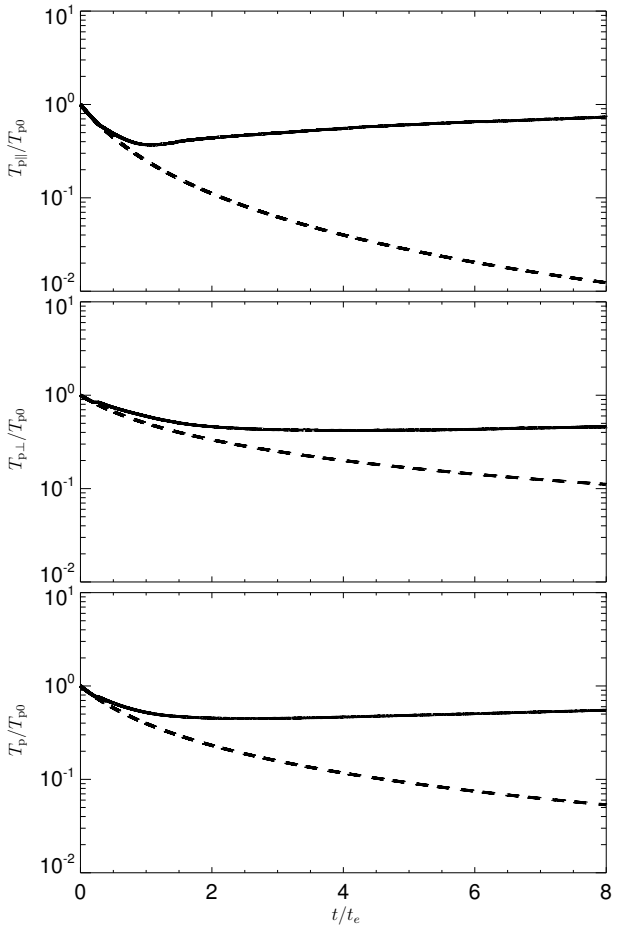

Figure 6. The parallel $T_{\mathrm{p}\parallel}$ (top), perpendicular $T_{\mathrm{p}\perp}$ (middle), and total T_{p} (bottom) temperatures of solar wind protons as functions of time. The dashed curves show the double-adiabatic prediction on the the top and middle panels. On the bottom panel the dashed curve shows the adiabatic prediction.

the velocities of the neutralized solar wind protons. Figure 7 shows the velocity distribution function f_{n} of the cumulated hot neutrals of the solar wind origin at the end of the simulation: The left panel displays f_{n} as a function of the radial component of the velocity v_R and the component parallel to the ambient magnetic field $v_\parallel$. The right panels shows f_{n} as a function of v_R and the component of the velocity perpendicular both the radial direction and the ambient magnetic field $v_{\perp 1}$. The two 2D projections indicate that the 3D velocity distribution function of hot neutrals is rather complex. The distribution is elongated along the radial direction owing to the overall deceleration of the solar wind plasma due to the injection of pick-up protons. The different profiles of the distribution in $v_\parallel$ and $v_{\perp 1}$ is a result of generally anisotropic proton velocity distribution function evolving differently in the direction parallel and perpendicular to the ambient magnetic field.

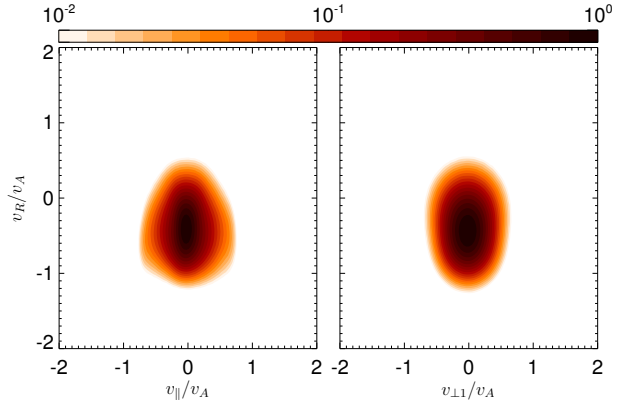

Figure 7. Distribution functions of the hot neutral hydrogen of the solar wind origin at the end of the simulations: f_{n} as a function of $v_\parallel$ and v_R (left panel) and f_{n} as a function of $v_{\perp 1}$ and v_R (normalized to their maximum value). The color scale is shown on the top.

4. DISCUSSION

We investigated effects of continuous injection of pick-up protons in the distant solar wind using 1-D hybrid expanding box model. We assumed an ideal 1-D homogeneous system parallel to the ambient magnetic field directed along the transverse direction with respect to the radial direction. We assumed a slowly expanding ($t_e = 10^4 \omega_{\mathrm{cp0}}^{-1}$) in the two transverse directions and a slow continuous injection of cold pick-up protons due to the charge-exchange process with the solar wind protons ($t_{cx} = 100 t_e$). The injection of pick-up protons leads to the formation of a ring velocity distribution distribution. This distribution becomes rapidly unstable and generates AIC waves that scatter through the cyclotron resonance the pick-up protons which consequently form

a shell velocity distribution distribution. The AIC waves also scatter the solar wind protons and heat them in the perpendicular direction and cool them in the parallel one. The continuous injection of pick-up protons keep the instability active, and, at later times, the AIC waves grow slowly (secularly, about linearly in time). The AIC waves become eventually unstable with respect to a parametric instability that leads to formation of a secondary, shorter wavelength population of AIC waves and compressible ion-acoustic waves. The ion-acoustic waves interact with solar wind protons through the Landau resonance. The combined effect of the AIC and ion-acoustic waves lead to an efficient proton parallel and perpendicular heating. The pick-up proton shell distribution thickens during the evolution due to diffusion owing to the AIC waves and due to the expansion driven cooling; eventually, a power-law distribution is expected with a cut off near the injection velocity. The pick-up proton generated AIC waves and the ion-acoustic waves generated by the parametric instabilities may be partly responsible for the enhanced level of density fluctuations observed in the outer heliosphere (Bellamy et al. 2005; Zank et al. 2012).

In the presented simulation we initialized the solar wind protons with $\beta_{\rm p} = 0.2$. To test the sensitivity of the simulation results with respect to $\beta_{\rm p}$ we performed additional simulations with $\beta_{\rm p} = 0.1$ and 1. For higher solar wind proton beta the cyclotron perpendicular heating becomes less efficient but overall behavior remain the same. For higher $\beta_{\rm p}$ one expects that the mirror instability would become important (Gary et al. 1997) and, also, properties of the parametric instabilities depend on $\beta_{\rm p}$ (Hollweg 1994). Therefore, the present results are relevant for $\beta_{\rm p} \lesssim 1$.

The present model is in many respects simplified, only one dimension is considered, the solar wind velocity is assumed to be constant and is about ten time faster than in the reality. Also, the system is assumed homogeneous, no pre-existing fluctuations/turbulence is assumed, Coulomb collisions and electron impact ionization are neglected, etc. However, the model self-consistently describes the kinetic plasma behavior in the expanding solar wind where pick-up protons are continuously injected.

The one-dimensional geometry strongly reduces the available physics, only parallel propagating modes are allowed. In a low beta plasma the ring is expected to generate cyclotron waves primarily along the magnetic field which justifies the 1-D geometry but other instabilities (such as the mirror instability) may appear at oblique angles and may modify the nonlinear behavior. Also the 1-D geometry tend to leads to larger amplitude fluctuations the are prone to parametric instabilities. At 2-D and 3-D the effect of parametric instabilities will be likely reduced.

The numerical resolution of the code could be source of other problems; our choice of the spatial grid, the box size, and the time step guaranties a good resolution of the AIC waves. While the used number of particles per cell is substantial (note that at $t = t_e$ there are about 10^3 particles per cell for pickup protons) the resulting numerical noise may lead to enhanced scattering of the ring pick-up protons. (Florinski et al. 2016). This is likely a minor problem since the continuous injection of pickup ions tends to keep the system unstable and rapidly generates fluctuations well above the numerical noise level.

The presence of large scale fluctuations/turbulence will modify the initial local pick-up ion distribution function and the resulting instabilities (Zank & Cairns 2000). For injection at nearly parallel angles with respect to the magnetic field beam-type instabilities are expected (Gary 1993). These instabilities have different nonlinear properties but quite generally one expects formation of partial spherical shells (cf., Williams & Zank 1994; Matteini et al. 2015).

Coulomb collisions are expected to be weak in the solar wind but may lead at the expansion time scale to scattering of pick-up ions (via interaction with the solar wind ions, cf., Tracy et al. 2015; Hellinger 2016) reducing thus the source of free energy for instabilities. Electron impact ionization is expected to have generally a subdominant effect with respect to the charge-exchange process in the solar wind (but it is likely important in the heliosheath, cf., Decker et al. 2008). This process would have a similar effect as the charge exchange (i.e., generation of pick-up ions) but without the reduction of the solar wind ion density. We expect the overall effect of electron impact ionization would comparable to that of charge exchange.

The connection between instabilities driven by the pick-up ions and turbulence remains an important open question. The turbulent fluctuations (or another wave activity) already present in the solar wind would scatter the pick-up ions and possibly reduce the source of free energy for instabilities. On the other hand, instabilities driven by pick-up ion ring-beam velocity distribution function generate typically waves at short, ion scales, often at nearly parallel angles with respect to the ambient magnetic field. Coupling between the strongly oblique turbulent fluctuations and quasi-parallel waves at ion scales is likely weak (while waves generated at strongly oblique angles seem to participate in the cascade, cf., Hellinger et al. 2015). There are many open problems that will be subject of future work.

In concluding, the present work shows that (i) collisionless plasma with energetically important population of pick-up ions generally needs a fully kinetic treatment, (ii) pick-up ion generated waves are able to directly quite efficiently heat the solar wind protons, (iii) the distribution function of pick-up ions at later times/larger distances has a wide spread of velocities/energies owing to scattering of the initial distribution on the generated waves and to the expansion-driven cooling, (iv) the hot neutrals of the solar wind origin have a complex velocity distribution function since they are neutralized at different distances and the solar wind ion temperature and the bulk velocity vary substantially over the time/distance.

REFERENCES

Adhikari, L., Zank, G. P., Bruno, R., Telloni, D., Hunana, P., Dosch, A., Marino, R., & Hu, Q. 2015, ApJ, 805, 63

Aggarwal, P., et al. 2016, ApJ, 822, 94

Araneda, J. A., Marsch, E., & Viñas, A. F. 2008, Phys. Rev. Lett., 100, 125003

Bellamy, B. R., Cairns, I. H., & Smith, C. W. 2005, J. Geophys. Res., 110, A10104

Burlaga, L. F., Ness, N. F., Acuña, M. H., Lepping, R. P., Connerney, J. E. P., & Richardson, J. D. 2008, Nature, 454, 75

Burlaga, L. F., Ness, N. F., Belcher, J. W., Lazarus, A. J., & Richardson, J. D. 1996, Space Sci. Rev., 78, 33

Cannon, B. E., Smith, C. W., Isenberg, P. A., Vasquez, B. J., Joyce, C. J., Murphy, N., & Nuno, R. G. 2014a, ApJ, 787, 133
Cannon, B. E., Smith, C. W., Isenberg, P. A., Vasquez, B. J., Murphy, N., & Nuno, R. G. 2014b, ApJ, 784, 150
Chew, G. F., Goldberger, M. L., & Low, F. E. 1956, Proc. R. Soc. London, A236, 112
Cowee, M. M., Russell, C. T., & Strangeway, R. J. 2008, J. Geophys. Res., 113, A08220
Daughton, W., & Gary, S. P. 1998, J. Geophys. Res., 103, 20613
Decker, R. B., Krimigis, S. M., Roelof, E. C., Hill, M. E., Armstrong, T. P., Gloeckler, G., Hamilton, D. C., & Lanzerotti, L. J. 2008, Nature, 454, 67
Florinski, V., Heerikhuisen, J., Niemiec, J., & Ernst, A. 2016, ApJ, 826, 197
Florinski, V., Zank, G. P., Heerikhuisen, J., Hu, Q., & Khazanov, I. 2010, ApJ, 719, 1097
Fraternale, F., Gallana, L., Iovieno, M., Opher, M., Richardson, J. D., & Tordella, D. 2016, Phys. Scripta, 91, 023011
Gary, S. P. 1993, Theory of Space Plasma Microinstabilities (New York: Cambridge Univ. Press)
Gary, S. P., Wang, J., Winske, D., & Fuselier, S. A. 1997, J. Geophys. Res., 102, 27159
Giacalone, J., & Decker, R. 2010, ApJ, 710, 91
Grappin, R., Velli, M., & Mangeney, A. 1993, Phys. Rev. Lett., 70, 2190
Gray, P. C., Smith, C. W., Matthaeus, W. H., & Otani, N. F. 1996, Geophys. Res. Lett., 23, 113
Hellinger, P. 2016, ApJ, 825, 120
Hellinger, P., Matteini, L., Landi, S., Verdini, A., Franci, L., & Trávníček, P. M. 2015, ApJL, 811, L32
Hellinger, P., & Trávníček, P. 2005, J. Geophys. Res., 110, A04210
Hellinger, P., Trávníček, P., Mangeney, A., & Grappin, R. 2003, Geophys. Res. Lett., 30, 1211
Hollweg, J. V. 1994, J. Geophys. Res., 99, 23431
Hollweg, J. V., & Isenberg, P. A. 2002, J. Geophys. Res., 107, 1147
Isenberg, P. A., Smith, C. W., & Matthaeus, W. H. 2003, ApJ, 592, 564
Isenberg, P. A., Smith, C. W., Matthaeus, W. H., & Richardson, J. D. 2010, ApJ, 719, 716
Joyce, C. J., Smith, C. W., Isenberg, P. A., Murphy, N., & Schwadron, N. A. 2010, ApJ, 724, 1256
Kunz, M. W., Schekochihin, A. A., & Stone, J. M. 2014, Phys. Rev. Lett., 112, 205003
Lee, M. A., & Ip, W.-H. 1987, J. Geophys. Res., 92, 11041
Liewer, P. C., Velli, M., & Goldstein, B. E. 2001, J. Geophys. Res., 106, 29261
Matsukiyo, S., & Scholer, H. 2014, J. Geophys. Res., 119, 2388
Matteini, L., Landi, S., Hellinger, P., & Velli, M. 2006, J. Geophys. Res., 111, A10101
Matteini, L., Landi, S., Velli, M., & Hellinger, P. 2010, J. Geophys. Res., 115, A09106
Matteini, L., Schwartz, S. J., & Hellinger, P. 2015, Planet. Space Sci., 119, 3
Matthaeus, W. H., Zank, G. P., Smith, C. W., & Oughton, S. 1999, Phys. Rev. Lett., 82, 3444
Matthews, A. 1994, J. Comput. Phys., 112, 102
Richardson, J. D., Liu, Y., Wang, C., & McComas, D. J. 2008, A&A, 491, 1
Richardson, J. D., Paularena, K. I., Lazarus, A. J., & Belcher, J. W. 1995, Geophys. Res. Lett., 22, 1469
Richardson, J. D., Phillips, J. L., Smith, C. W., & Gray, P. C. 1996, Geophys. Res. Lett., 23, 3259
Richardson, J. D., & Stone, E. D. 2009, Space Sci. Rev., 143, 7
Rosin, M. S., Schekochihin, A. A., Rincon, F., & Cowley, S. C. 2011, MNRAS, 413, 7
Smith, C. W., Isenberg, P. A., Matthaeus, W. H., & Richardson, J. D. 2006, ApJ, 638, 508
Tracy, P. J., Kasper, J. C., Zurbuchen, T. H., Raines, J. M., Shearer, P., & Gilbert, J. 2015, ApJ, 812, 170
Usmanov, A. V., Goldstein, M. L., & Matthaeus, W. H. 2012, ApJ, 754, 40
Vandas, M., & Hellinger, P. 2015, Phys. Plasmas, 22, 062107
Vasquez, B. J. 1995, J. Geophys. Res., 100, 1779
Wang, C., Richardson, J. D., & Gosling, J. T. 2000, Geophys. Res. Lett., 27, 2429
Williams, L. L., & Zank, G. P. 1994, J. Geophys. Res., 99, 19229
Yang, Z., Liu, Y. D., Richardson, J. D., Lu, Q., Huang, C., & Wang, R. 2015, ApJ, 809, 28
Zank, G. P., & Cairns, I. H. 2000, ApJ, 541, 489
Zank, G. P., Hunana, P., Mostafavi, P., & Goldstein, M. L. 2014, ApJ, 797, 87
Zank, G. P., Jetha, N., Hu, Q., & Hunana, P. 2012, ApJ, 756, 21
Zank, G. P., Pauls, H. L., Cairns, I. H., & Webb, G. M. 1996, J. Geophys. Res., 101, 457
Zank, G. P., Pogorelov, N. V., Heerikhuisen, J., Washimi, H., Florinski, V., Borovikov, S., Kryukov, I., & Müller, H. R. 2009, Space Sci. Rev., 146, 295